In Vivo Bioluminescence Imaging in a Rabbit Model of Orthopaedic Implant-Associated Infection to Monitor Efficacy of an Antibiotic-Releasing Coating

Robert J. Miller, MS, John M. Thompson, MD, Jesse Zheng, BS, Mark C. Marchitto, MD, Nathan K. Archer, PhD, Bret L. Pinsker, BS, Roger V. Ortines, MS, Xuesong Jiang, PhD, Russell A. Martin, PhD, Isabelle D. Brown, BS, Yu Wang, PhD, Robert S. Sterling, MD, Hai-Quan Mao, PhD, and Lloyd S. Miller, MD, PhD

Investigation performed at the Johns Hopkins University School of Medicine, Baltimore, Maryland

Background: In vivo bioluminescence imaging (BLI) provides noninvasive monitoring of bacterial burden in animal models of orthopaedic implant-associated infection (OIAI). However, technical limitations have limited its use to mouse and rat models of OIAI. The goal of this study was to develop a larger, rabbit model of OIAI using in vivo BLI to evaluate the efficacy of an antibiotic-releasing implant coating.

Methods: A nanofiber coating loaded with or without linezolid-rifampin was electrospun onto a surgical-grade locking peg. To model OIAI in rabbits, a medial parapatellar arthrotomy was performed to ream the femoral canal, and a bright bioluminescent methicillin-resistant *Staphylococcus aureus* (MRSA) strain was inoculated into the canal, followed by retrograde insertion of the coated implant flush with the articular surface. In vivo BLI signals were confirmed by ex vivo colony-forming units (CFUs) from tissue, bone, and implant specimens.

Results: In this rabbit model of OIAI (n = 6 rabbits per group), implants coated without antibiotics were associated with significantly increased knee width and in vivo BLI signals compared with implants coated with linezolid-rifampin ($p < 0.001$ and $p < 0.05$, respectively). On day 7, the implants without antibiotics were associated with significantly increased CFUs from tissue (mean [and standard error of the mean], $1.4 \times 10^8 \pm 2.1 \times 10^7$ CFUs; $p < 0.001$), bone ($6.9 \times 10^6 \pm 3.1 \times 10^6$ CFUs; $p < 0.05$), and implant ($5.1 \times 10^5 \pm 2.2 \times 10^5$ CFUs; $p < 0.05$) specimens compared with implants with linezolid-rifampin, which demonstrated no detectable CFUs from any source.

Conclusions: By combining a bright bioluminescent MRSA strain with modified techniques, in vivo BLI in a rabbit model of OIAI demonstrated the efficacy of an antibiotic-releasing coating.

Clinical Relevance: The new capability of in vivo BLI for noninvasive monitoring of bacterial burden in larger-animal models of OIAI may have important preclinical relevance.

Orthopaedic implant-associated infections (OIAIs) are serious complications in orthopaedic surgery[1-3]. Periprosthetic joint infections (PJIs) occur in 1% to 2% of primary and 3% to 6% of revision arthroplasties[4-6], and infection in open fractures treated with intramedullary nailing occurs in up to 30% of cases[7,8]. These percentages correspond to ~25,000 PJIs and ~100,000 fracture-fixation device-related infections in the U.S. annually[9,10], which are increasing with clinical demand[11].

In vivo bioluminescence imaging (BLI) provides the opportunity of noninvasive monitoring of the bacterial burden in animal models of OIAI to study pathogenesis[12-20], diagnosis[21,22], and treatments[23-33]. This technology employs bioluminescent bacteria engineered with a *lux* operon, resulting in light

Disclosure: This work was supported by a Johns Hopkins University-Coulter Translational Partnership Award (R.S.S., H-Q.M., and L.S.M.) and T32 AR07708-01 from the National Institute of Arthritis and Musculoskeletal and Skin Diseases of the U.S. National Institutes of Health (J.M.T.). The coating investigated in this work is included in a pending U.S. patent application serial no. 16/076,606: "Compositions and Methods for Preparation of Composite Polymer Coatings on Medical Implants, and Their Use for Co-delivery of Multiple Antimicrobial Agents" (J.Z., H.-Q.M., and L.S.M.). On the **Disclosure of Potential Conflicts of Interest** forms, *which are provided with the online version of the article*, one or more of the authors checked "yes" to indicate that the author had a relevant financial relationship in the biomedical arena outside the submitted work and "yes" to indicate that the author had a patent and/or copyright, planned, pending, or issued, broadly relevant to this work (http://links.lww.com/JBJS/F59).

emission from live and actively metabolizing bacteria that can be measured by an in vivo imaging system (IVIS)[34]. However, insufficient bacterial light production, poor light penetration through deep tissues, and IVIS machines that are configured for rodents have limited in vivo BLI to mouse and rat models of OIAI[34]. Highlighting this limitation, BLI could only be performed post mortem in a rabbit knee-joint OIAI model after removal of overlying musculoskeletal tissues and opening of the joint capsule[35].

If in vivo BLI could be expanded to larger-animal models of OIAI in which complex orthopaedic surgical procedures and implants can be used, clinical relevance may be greatly improved[36,37]. This prompted us to develop a rabbit model of OIAI in which in vivo BLI was used to assess the preclinical efficacy of an antibiotic-releasing implant coating that was previously demonstrated to be effective in a mouse model of OIAI[23].

Materials and Methods

Antibiotic-Loaded Implant Coating

To generate a poly(D,L-lactic-co-glycolic acid) (PLGA) and poly(ε-caprolactone) (PCL) nanofiber coating loaded without (designated "−/−") or with (linezolid [Lin] in PLGA and PCL and rifampin [Rif] in PCL, designated "Lin/Lin + Rif") antibiotics, previous methods were modified[23]. Rifampin was used in combination with linezolid to prevent the development of rifampin-resistant bacteria if rifampin were to be used alone. First, orthopaedic-grade titanium locking pegs (2 × 24 mm; Zimmer Biomet) were etched by incubating in 5 M NaOH solution at 37°C for 8 hours (Fig. 1). After rinsing with deionized water and drying in a lyophilizer for 24 hours, implants were dipped (insertion/removal speed of 0.25 cm/sec) in a solution of poly(L-lactic acid) (PLA polymer 6201D; NatureWorks) dissolved in dichloromethane (10.0 w/w%). PLGA (75:25, molecular weight [MW] 66,000 to 107,000) was dissolved in hexafluoro-2-propanol (10.0 w/w%) ± linezolid (1.0 w/w%) (all Sigma-Aldrich). PCL (MW 200,000; PolySciTech) was dissolved in dichloromethane and isopropanol (75:25, 5.0 w/w%; Sigma-Aldrich) ± linezolid (0.1 w/w%; Santa Cruz Biotechnology), rifampin (0.5 w/w%; Sigma-Aldrich), and NaCl (0.1 w/w%). For co-electrospinning, solutions of PLGA and PCL were loaded into separate 1-mL syringes fitted with blunt-end 27-gauge needles. High-power voltage sources were connected via alligator clips to each needle tip and supplied with 6 to 7-kV voltage between the needles and the implant. Two syringe pumps were used to feed the PLGA (25 mL/hr) and PCL (1.5 mL/hr) polymer solutions. PLGA and PCL nanofibers were collected simultaneously and directly onto the grounded etched/PLA-coated implants at a distance of 10 cm with the implants held by a rotary tool grip at each distal end for 8 and 7 minutes, respectively. Co-electrospinning was performed to coat the implants with PLGA and PCL nanofibers loaded with or without antibiotics. The coated implants were annealed for 15 minutes at 70°C to generate a conformal PCL and PLGA fiber coating; residual solvent was removed by overnight lyophilization.

Scanning Electron Microscopy

The implants were sputter-coated with gold-palladium alloy and imaged with a field-emission scanning electron microscope (JSM-6700F field-emission scanning electron microscope [FE-SEM]; JEOL) (Fig. 1), as previously described[23].

In Vitro Antibiotic Release

Implants with the antibiotic-loaded coatings were submerged in 1 mL of phosphate-buffered saline (PBS) solution (pH 7.4) at 37°C, and the drug-release medium was changed daily for 18 days and stored at −20°C. Antibiotic concentrations in the drug-release media were quantified by high-performance liquid chromatography (HPLC) using wavelengths for linezolid (254 nm) and rifampin (263 mm), as previously described[23].

Bacteria

The bioluminescent *Staphylococcus aureus* strain SAP231 (provided by Roger Plaut, U.S. Food and Drug Administration [FDA]) possesses a stably integrated *lux* construct in the bacterial chromosome previously generated from the NRS384 methicillin-resistant *S. aureus* (MRSA) strain[38]. SAP231 was streaked onto tryptic soy agar (TSA) plates and incubated overnight at 37°C. Individual colonies were cultured in tryptic soy broth (TSB) overnight at 37°C with shaking (240 rpm). A 1:50 dilution of the overnight culture was subcultured for 2 hours at 37°C with shaking, and bacteria were washed in PBS solution and reconstituted to an inoculum of 1×10^4 CFUs (colony-forming units) in 10 μL of PBS solution as determined by absorbance at 600 nm (A_{600}) and confirmed by overnight culture on plates.

In Vitro Antimicrobial Assay

Mid-logarithmic-phase SAP231 was prepared as above and diluted to 1×10^3 CFU/mL in Cation-Adjusted Mueller Hinton II Broth (Becton Dickinson), pH 7.3. Bacteria were cultured 1:1, with drug-release media collected daily (see above) for 18 days at 37°C, and CFUs were enumerated by absorbance (A_{600}) and a CFU standard curve.

Rabbit Model of OIAI

All procedures were approved by the Johns Hopkins Animal Care and Use Committee. A sample size of 6 rabbits per group was chosen for this proof-of-concept study. Ten to 16-week-old male Dutch Belted rabbits (Robinson Services) (~2 kg body weight) were anesthetized via intramuscular injection of a mixture of ketamine (25 mg/kg) and xylazine (1.5 mg/kg) (ZooPharm), and maintained with isoflurane (1.5%). Sterile ophthalmic ointment (Rugby) was applied to the eyes.

For each rabbit, sustained-release buprenorphine (ZooPharm) (0.2 mg/kg) and sustained-release meloxicam (Norbrook Laboratories) (0.6 mg/dose) were injected subcutaneously for analgesia. Metoclopramide (Teva) (0.3 mg/kg) was injected subcutaneously as a gastrointestinal promotility agent. The distal anterior region of the right thigh through the proximal aspect of the leg was shaved and prepared with isopropyl alcohol (70%) followed by povidone-iodine (10%), each

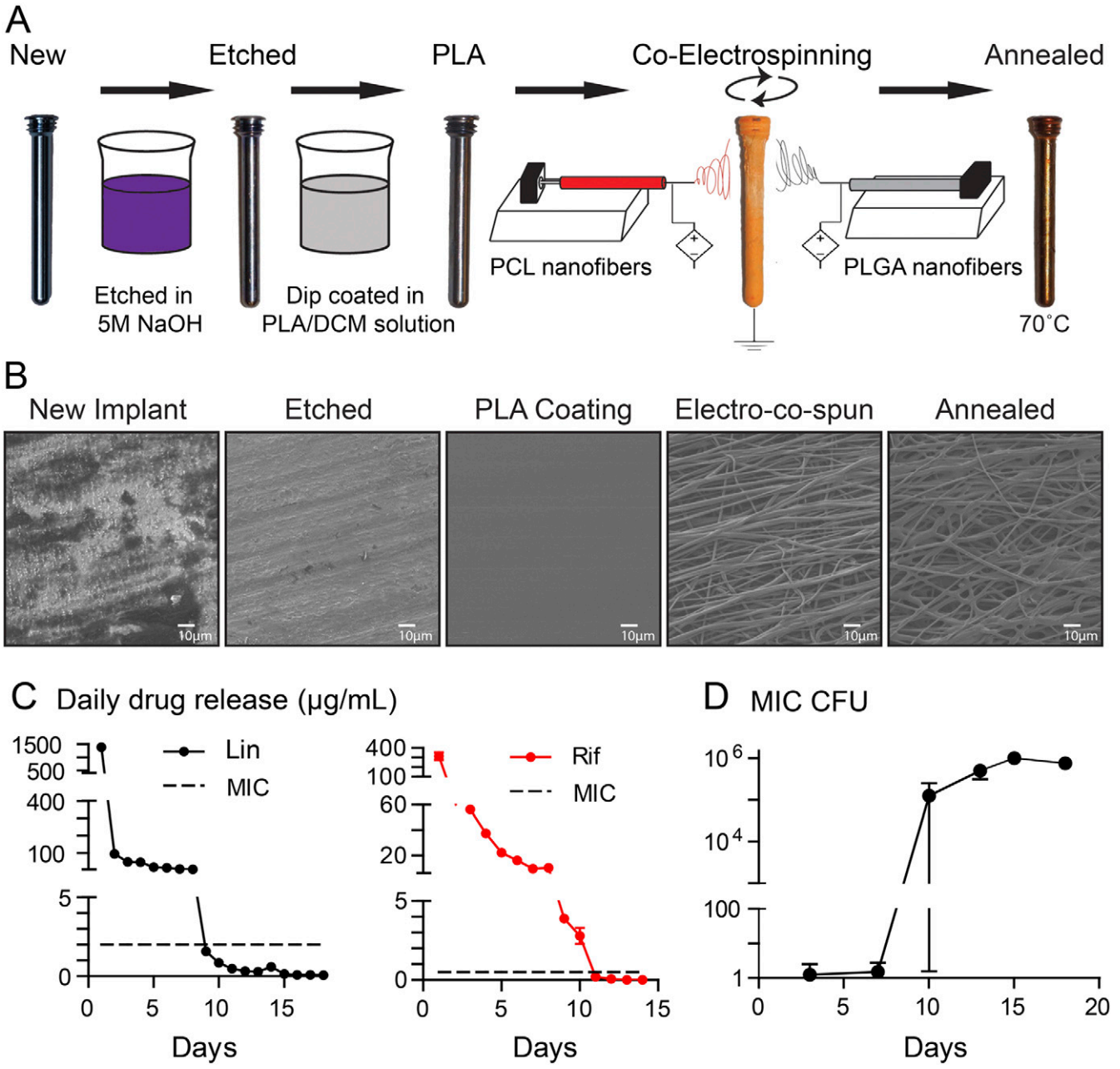

Fig. 1

Figs. 1-A through 1-D Antibiotic-loaded implant coating. **Fig. 1-A** The nanofiber antibiotic-releasing coating was prepared using base-etched orthopaedic-grade titanium peg implants, which were then dip-coated in PLA dissolved in dichloromethane (PLA/DCM) solution. Co-electrospinning was performed to coat the implants with PLGA and PCL nanofibers loaded with or without antibiotics followed by heat treatment (annealing) to generate a conformal PCL and PLGA fiber coating. **Fig. 1-B** Representative scanning electron microscopy images of the implant and nanofiber coating surfaces after each step in the coating process. **Fig. 1-C** In vitro antibiotic release of linezolid (Lin) or rifampin (Rif) (mean µg/mL and SEM) measured by placing the coated implants into a new solution of PBS daily for 18 days (n = 6 coated implants per group). The horizontal dotted lines show the minimum inhibitory concentration (MIC) of SAP231 for Lin (2 µg/mL) and Rif (0.5 µg/mL). **Fig. 1-D** In vitro antimicrobial activity assays were performed by incubating the drug-release media from the Lin/Lin + Rif-coated implants collected daily and analyzed on days 3, 7, 10, 13, 15, and 18. CFUs (mean and SEM, logarithmic scale) were enumerated by absorbance (A_{600}) and a CFU standard curve for the coatings (n = 6 coated implants per group).

applied 3 times (Fig. 2-A). In slight knee flexion, a midline incision and a medial parapatellar arthrotomy were performed (Fig. 2-B), and the patella was dislocated laterally to expose the trochlea and intercondylar notch (Fig. 2-C). In maximal knee flexion, a 2-mm drill-bit was used to access the femoral canal just anterior to the Blumensaat line (Fig. 2-D), and a 2.2-mm

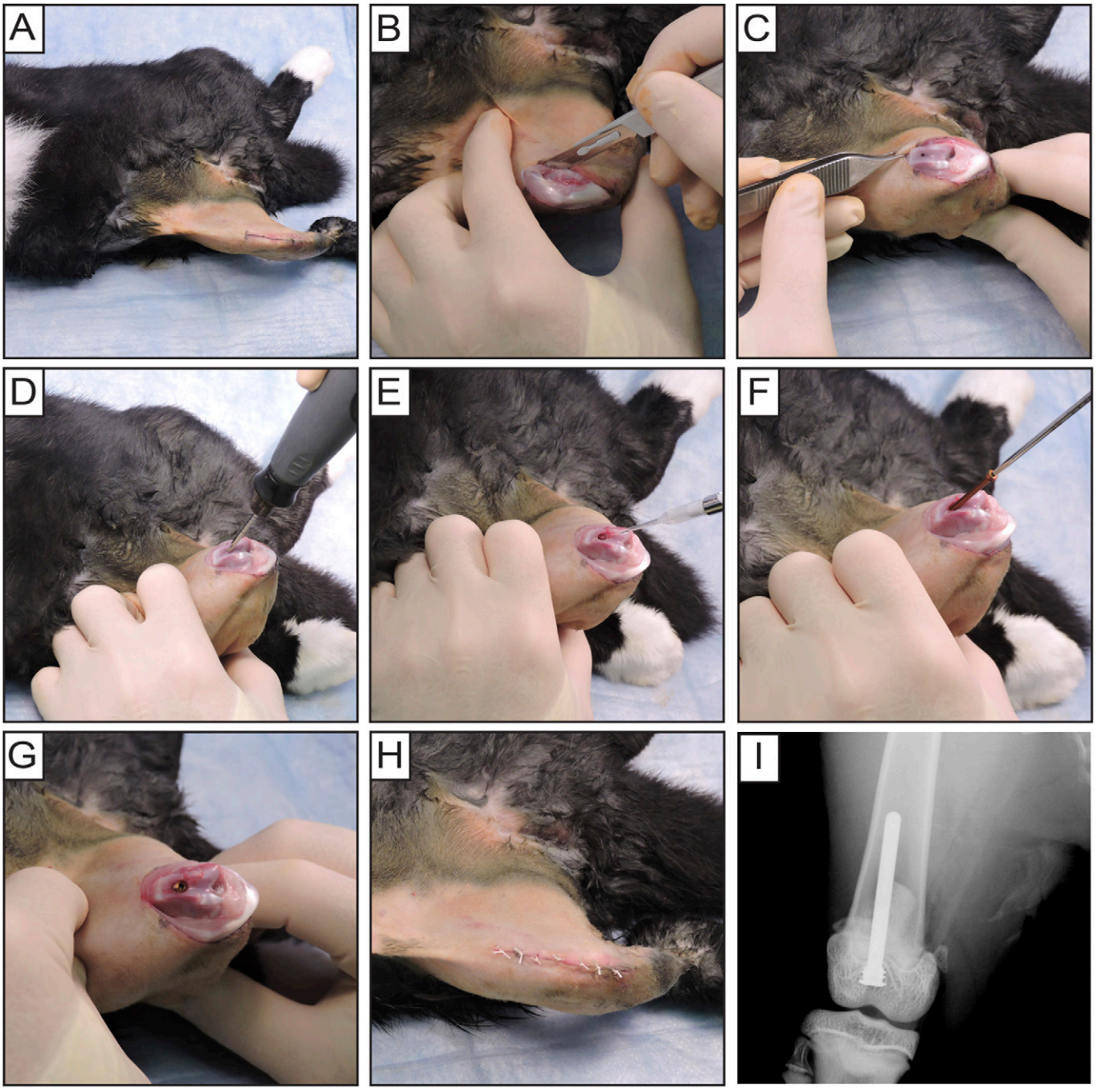

Fig. 2

Figs. 2-A through 2-I Rabbit surgical procedures. **Fig. 2-A** The distal anterior region of the right thigh through the proximal aspect of the leg was shaved and prepared. **Fig. 2-B** After a midline incision was made over the patella, a medial parapatellar arthrotomy was performed. **Fig. 2-C** The patella was dislocated laterally to expose the trochlea and intercondylar notch. **Fig. 2-D** The femoral medullary canal was drilled and the implant was countersunk anterior to the intercondylar notch. **Fig. 2-E** *S. aureus* (bioluminescent strain SAP231, 1×10^4 CFUs in 10 μL of PBS solution) was pipetted into the canal. **Fig. 2-F** Coated implants were manually inserted retrograde with a screwdriver. **Fig. 2-G** Implant flush with the articular surface. **Fig. 2-H** The patella was relocated and the surgical site was closed with sutures. **Fig. 2-I** Anteroposterior radiographic image of implant placement.

drill-bit was used to countersink the implant. SAP231 (1×10^4 CFUs in 10 μL PBS solution) was pipetted into the canal (Fig. 2-E). The coated implant was manually placed through retrograde insertion with a screwdriver until flush with the articular surface (Figs. 2-F and 2-G). The patella was relocated and the surgical site closed in layered fashion with interrupted 4-0

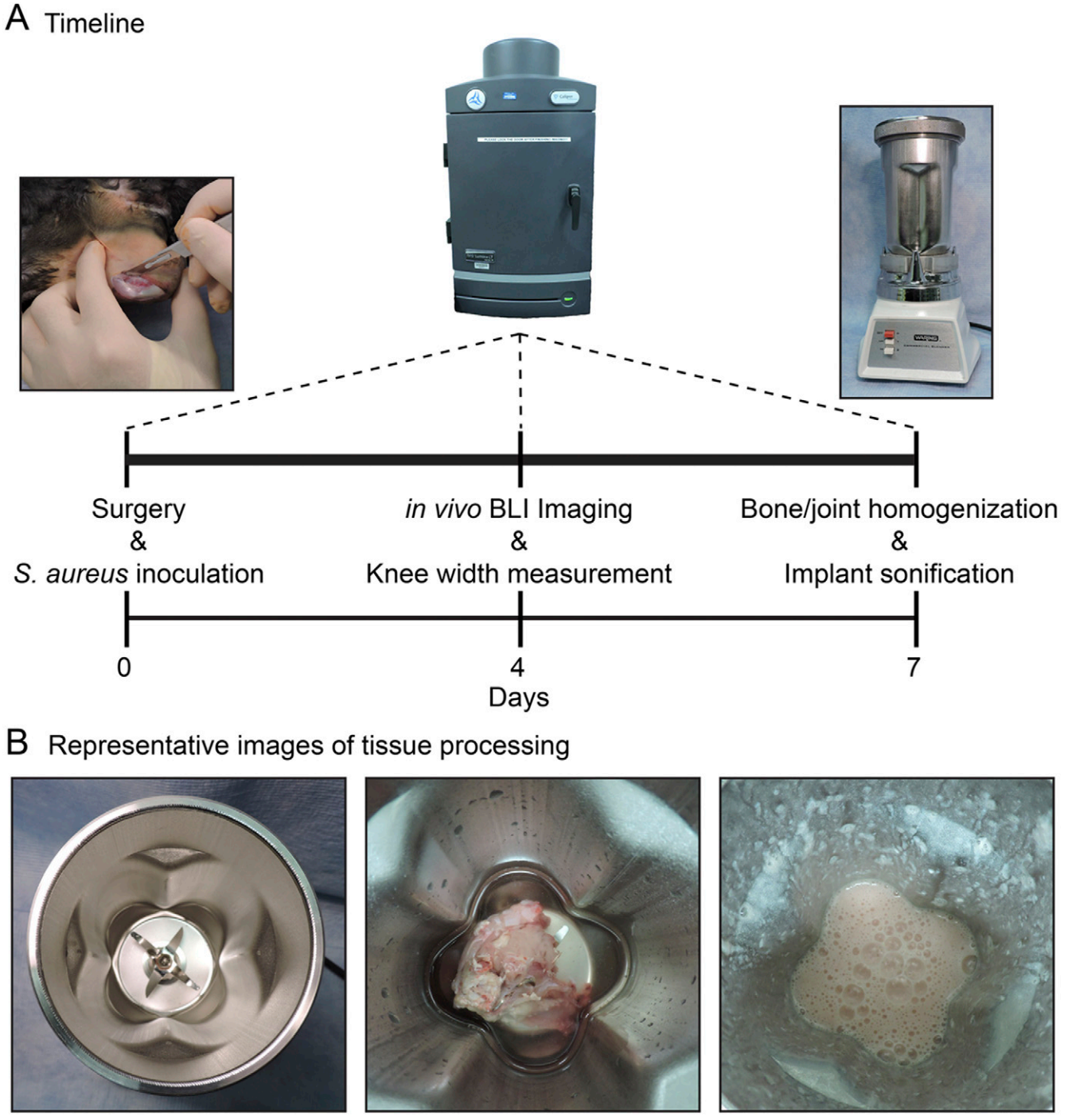

Fig. 3

Figs. 3-A and 3-B Timeline and representative images of tissue processing. **Fig. 3-A** Timeline of the rabbit model of orthopaedic implant-associated infection with surgery and inoculation performed on day 0, in vivo BLI and knee-width measurements performed on anesthetized rabbits on days 0, 4, and 7, and muscle/tendon tissue, bone, and implant specimens harvested and processed on day 7 to determine ex vivo CFUs. **Fig. 3-B** Representative images of the tissue processing, with the empty blender cartridge (left panel), placement of a muscle/tendon specimen in the blender (middle panel), and the appearance of liquid homogenates after blending (right panel). Similar procedures were used for homogenizing the bone specimens.

Vicryl sutures (Ethicon) (Fig. 2-H). An anteroposterior radiograph (1 per rabbit) confirmed implant placement (Faxitron MX-20; Faxitron Bioptics) (Fig. 2-I).

In Vivo BLI

Each rabbit was anesthetized via intramuscular injection of ketamine (25 mg/kg) and xylazine (1.5 mg/kg) (ZooPharm)

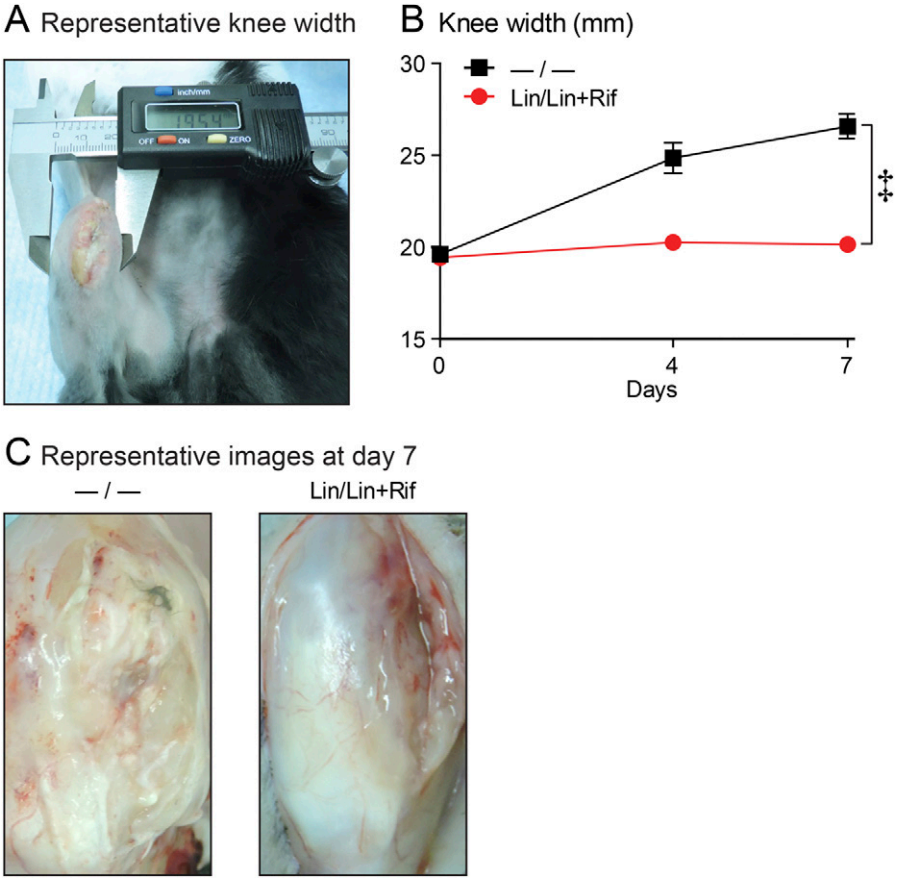

Fig. 4

Figs. 4-A, 4-B, and 4-C Knee-width measurement. The rabbit model of orthopaedic implant-associated infection involved the surgical placement of coated implants without (−/−) or with (Lin/Lin + Rif) antibiotics (n = 6 rabbits per experimental group). **Fig. 4-A** Representative photograph of caliper measurement of knee width. **Fig. 4-B** Mean knee width (in mm) and standard error of the mean (see also Table I). ‡P < 0.001, Lin/Lin + Rif versus −/−, as calculated by 2-way ANOVA. **Fig. 4-C** Representative knee-tissue appearance on day 7, after overlying skin was removed.

and positioned semi-upright in the IVIS Lumina III chamber (PerkinElmer), with the postoperative right knee almost maximally flexed and positioned underneath the CCD (charge-coupled device) camera. In vivo BLI signals were acquired (5-minute exposure and medium binning), overlaid onto a grayscale photograph, and quantified as total flux (photons/sec) within

TABLE I Knee Width Data in Figure 4-B and in Vivo Bioluminescence Imaging (BLI) Data in Figure 5-B*

	Mean and SEM			
	Day 0	Day 4	Day 7	P Value†
Knee width *(mm)*				<0.001
—/—	19.61 ± 0.25	24.85 ± 0.82	26.58 ± 0.67	
Lin/Lin + Rif	19.43 ± 0.30	20.26 ± 0.40	20.15 ± 0.27	
In vivo BLI signals *(photons/sec)*				<0.05
—/—	$1.9 \times 10^5 \pm 5.0 \times 10^4$ (below LOD)	$3.8 \times 10^7 \pm 1.4 \times 10^7$	$3.5 \times 10^7 \pm 1.6 \times 10^7$	
Lin/Lin + Rif	$1.5 \times 10^5 \pm 4.2 \times 10^4$ (below LOD)	$1.1 \times 10^5 \pm 1.1 \times 10^4$ (below LOD)	$1.4 \times 10^5 \pm 3.8 \times 10^4$ (below LOD)	

*The rabbit model of orthopaedic implant-associated infection (OIAI) involved the surgical placement of coated implants without (−/−) or with (Lin/Lin + Rif) antibiotics. N = 6 rabbits per experimental group. Knee width and in vivo BLI were measured longitudinally on days 0, 4, and 7. SEM = standard error of the mean, and LOD = limit of detection (2×10^5 photons/sec). †Two-way ANOVA.

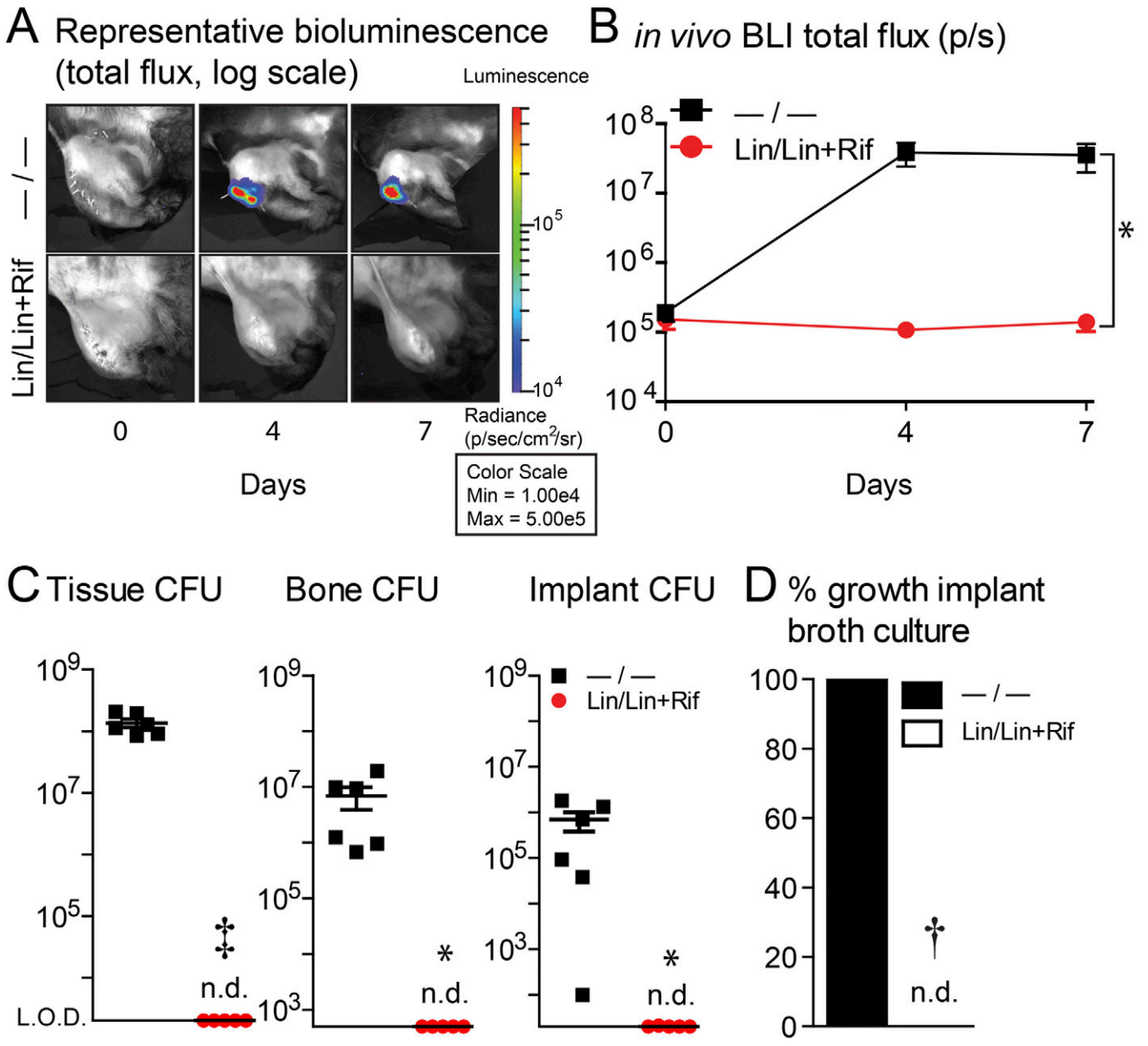

Fig. 5

Figs. 5-A through 5-D In vivo BLI. The rabbit model of orthopaedic implant-associated infection involved the surgical placement of coated implants without (−/−) or with (Lin/Lin + Rif) antibiotics (n = 6 rabbits per experimental group). *P < 0.05, †p < 0.01, and ‡p < 0.001, −/− versus Lin/Lin + Rif, as calculated by 2-way ANOVA (**Fig. 5-B**), 2-tailed Student t test (**Fig. 5-C**), or 2-tailed Fisher exact test (**Fig. 5-D**). n.d.= none detected. **Fig. 5-A** Representative in vivo BLI signals overlaid on a grayscale photograph of rabbit knees postoperatively. **Fig. 5-B** Bacterial burden as measured by in vivo BLI (in photons/sec) (mean and SEM, logarithmic scale) (see also Table I). LOD (limit of detection): 2×10^5 photons/sec (p/s). **Fig. 5-C** Ex vivo CFUs (mean and SEM, logarithmic scale) from muscle/tendon tissue, bone, and implant specimens (see also Table II). LOD = limit of detection (for tissue: 2×10^3 CFUs; bone: 5×10^2 CFUs; and implant: 2×10^1 CFUs). **Fig. 5-D** Percentage of implant sonicates with bacterial growth after culture in shaken broth for 48 hours followed by culture on plates for an additional 48 hours.

an oval region of interest (3 × 4 cm) using Living Image software (PerkinElmer).

Knee-Width Measurement

The postoperative knee was maximally flexed and the maximal medial-lateral width of the knee joint was measured manually with a Pittsburgh digital caliper (Harbor Freight Tools) by an investigator who was not blinded to the treatment group.

Ex Vivo CFU

On day 7, rabbits were killed and each muscle/tendon (i.e., muscle and tendon) tissue specimen was placed in a blender

container with 200 μL of PBS solution, each femur was manually crushed and placed in a blender container with 50 μL of PBS solution, and each implant was placed in a conical tube with 2 mL of TSB with 0.3% TWEEN 20 (Sigma-Aldrich). Each tissue and bone specimen was separately homogenized at 20,000 rpm for 30 to 120 seconds in a commercial blender (7011HS; Waring). To isolate bacteria adherent to the implants, each implant was vortexed for 2 minutes (10,000 rpm), sonicated for 10 minutes, and vortexed again for 2 minutes. Serial dilutions of each tissue homogenate or sonicate solution were plated and CFUs counted after overnight culture at 37°C. To detect *S. aureus* persisters and small-colony variants, each sonicate solution was incubated at 37°C with shaking (240 rpm) for an additional 48 hours, followed by another 48-hour culture on plates[39].

Statistical Analysis

Data were analyzed using Prism software (GraphPad) and are presented as the mean and standard error of the mean (SEM). Data were compared by a 2-tailed Student t test, 2-way analysis of variance (ANOVA), or 2-tailed Fisher exact test (see figure legends). P values of <0.05 were considered significant.

Results

Generation of an Antibiotic-Loaded Implant Coating

To generate an implant coating that releases antibiotics for at least 7 days, previous techniques were modified, as described above[23]. The implants were base-etched and dipped in PLA, co-electrospun with PLGA and PCL loaded with (Lin/Lin + Rif) or without (−/−) antibiotics, and annealed. In vitro analysis indicated that linezolid and rifampin were released above the minimum inhibitory concentration (MIC) for 8 to 10 days, and in vitro *S. aureus* growth was not observed until day 10 (Fig. 1).

Rabbit Model of OIAI

The rabbit model of OIAI was utilized whereby the right femoral canal was reamed followed by MRSA inoculation and placement of Lin/Lin + Rif or −/− coated implants (Fig. 2).

Timeline for BLI and CFU Enumeration

In vivo BLI was performed on anesthetized rabbits on days 0, 4, and 7. Rabbits were killed on day 7, and tissue and bone specimens were separately homogenized and implants were sonicated to assess ex vivo CFUs (Fig. 3).

Efficacy of the Antibiotic-Releasing Coating

To assess infection-induced inflammation, knee width was measured on days 0, 4, and 7 (Fig. 4-A). The −/− group demonstrated a 36% increase in knee width; this was significantly greater than that in the Lin/Lin + Rif group, which maintained the same knee width as that seen at baseline ($p < 0.001$) (Fig. 4-B and Table I). For assessment of the joint tissue, rabbits were killed on day 7 and the overlying skin was removed. The knee-joint tissue was purulent and friable in the −/− group, whereas it appeared normal in the Lin/Lin + Rif group (Fig. 4-C).

TABLE II Ex Vivo Colony-Forming Unit (CFU) Data in Figure 5-C*

	Mean CFUs and SEM	P Value†
Specimen source: tissue		<0.001
—/—	$1.4 \times 10^8 \pm 2.1 \times 10^7$	
Lin/Lin + Rif	None detected (below LOD)	
Specimen source: bone		<0.05
—/—	$6.9 \times 10^6 \pm 3.1 \times 10^6$	
Lin/Lin + Rif	None detected (below LOD)	
Specimen source: implant		<0.05
—/—	$5.1 \times 10^5 \pm 2.2 \times 10^5$	
Lin/Lin + Rif	None detected (below LOD)	

*The rabbit model of orthopaedic implant-associated infection (OIAI) involved the surgical placement of coated implants without (−/−) or with (Lin/Lin + Rif) antibiotics. N = 6 rabbits per experimental group. On day 7, the rabbits were killed and tissue (muscle/tendon), bone, and implant specimens were harvested and processed to determine ex vivo CFUs (mean and standard error of the mean [SEM]). LOD = limit of detection (for tissue: 2×10^3 CFUs; bone: 5×10^2 CFUs; implant: 2×10^1 CFUs). †Two-tailed Student t test.

In vivo BLI revealed high bacterial bioluminescent signals with the −/− coating on days 4 and 7 (peaking on day 4), with total flux values significantly greater than those of the Lin/Lin + Rif coating ($p < 0.05$), which remained below the limit of detection on all postoperative days (Figs. 5-A and 5-B and Table I). To confirm in vivo BLI data, rabbits were killed on day 7 and ex vivo CFUs enumerated. The rabbits with the −/− coating had increased CFUs isolated from the tissue ($p < 0.001$), bone ($p < 0.05$), and implant ($p < 0.05$) specimens compared with those with the Lin/Lin + Rif coating, which had undetectable CFUs from all sources (Fig. 5-C and Table II). Finally, sonicates from the implants were cultured for an additional 48 hours in broth followed by another 48 hours on plates to evaluate for any remaining *S. aureus* bacteria. All of the −/− coating sonicates had bacterial growth, whereas no bacterial growth was detected from Lin/Lin + Rif coating sonicates (Fig. 5-D).

Discussion

OIAI complications result in increased morbidity, mortality, and health-care costs and worse clinical outcomes[1-3]. Efforts to elucidate pathogenesis and enhance diagnosis and treatment have used preclinical models of OIAI, but current small-animal models lack complex procedures and surgical-grade implants, and in vivo BLI for monitoring infection has not been feasible in larger animals[36,37]. Herein, we described the development of a rabbit model of OIAI using in vivo BLI and demonstrated the efficacy of an antibiotic-releasing implant coating to prevent an MRSA OIAI.

To the best of our knowledge, this is the first larger-animal model of OIAI to incorporate in vivo BLI to non-invasively and longitudinally monitor the bacterial burden. This was accomplished by using a bright bioluminescent MRSA strain (SAP231) in which the *lux* operon was inserted into a

pseudogene under the control of a strong constitutively active promoter[38]. In mouse models of OIAI, the SAP231 strain produced in vivo BLI signals that were a log unit higher[31,33] than multiple other bioluminescent *S. aureus* strains[20]. In addition, for the rabbit OIAI model, we used Dutch Belted rabbits because the adults are small enough to fit within the standard chambers of existing IVIS machines.

This new capability is advantageous for the preclinical investigation of OIAI. First, this rabbit model of OIAI used a clinically applied orthopaedic implant, and the involvement of distinct tissue layers during the surgical approach and closure replicated a medial parapatellar arthrotomy in humans. Second, we chose an orthopaedic implant that was threaded within the intercondylar bone to reproduce the initially stable implants in clinical OIAI[40], which is an improvement over smooth Kirschner-wire implants commonly used in mouse models of OIAI[37]. Third, the use of in vivo BLI substantially reduces animal numbers because euthanasia at multiple time points is not required to obtain CFU data; minimizes pain and distress because invasive sampling techniques are not required to obtain tissue or joint fluid; and can be used to determine relevant time points for additional investigation. Fourth, *S. aureus* virulence factors such as Panton-Valentine leukocidin (PVL) are active in rabbits (and humans) but not in mice, suggesting that rabbits represent a more clinically relevant animal model for studying *S. aureus* infections[41]. Collectively, this rabbit OIAI model using in vivo BLI will permit preclinical evaluation of local and systemic antibiotics, biomaterials, and diagnostics in a larger animal model of OIAI, while reducing animal numbers and experimental costs for larger-animal studies.

We previously reported that a PLGA and PCL co-electrospun coating loaded with antibiotics (vancomycin, daptomycin, or linezolid combined with rifampin) prevented infection in a mouse model of OIAI[23]. PLGA and PCL are biocompatible, bioresorbable, and clinically used materials in sutures and drug-delivery devices[42,43]. We found that PLGA releases drugs more slowly than PCL, and various configurations of 1 or 2 (or multiple) antibiotics loaded onto each or both types of nanofibers can lead to different drug-elution concentrations and durations of release for optimal efficacy. Thus, the coating is highly versatile, and the polymers or drug concentrations could be modified for more rapid or longer release if desired[23]. Theoretically, any antibiotic that is heat-stable up to 65° to 70°C could be incorporated into this nanofiber coating, so it could provide coverage against monomicrobial and polymicrobial infections. The co-electrospinning coating technique is rapid and simple, requiring only a voltage source connected to the coating solutions to deliver them to a rotating implant, and can be applied to any metallic orthopaedic implant during the manufacturing process. An advance was made in which base-etching and adding a PLA primer prior to the co-electrospun PLGA and PCL coating were performed to enhance the coating durability to withstand the surgical procedures in the rabbit model.

There were limitations to our study. First, investigations involving rabbits might not fully translate to human OIAI. However, we used orthopaedic-grade implants, clinically relevant antibiotics, and PLGA and PCL polymers that are currently in clinical use[42,43]. Second, while the rabbit group size was small (n = 6 per group), it was sufficient to determine significance for all end points. Third, the in vivo BLI signals in the rabbit OIAI model likely corresponded to soft-tissue infection, as there were >10-fold and >100-fold greater ex vivo CFUs isolated from the tissue than from the bone and implant specimens, respectively. Furthermore, in vivo BLI signals are also affected by bacterial metabolic activity and growth that is higher when bacteria are in the tissue, as previously described for a mouse model of OIAI in which in vivo BLI signals peaked on postoperative days 2 to 4 during transition from planktonic to biofilm growth[17]. Finally, prolonging the study beyond 7 days could provide the opportunity to acquire insights into osteolysis or implant migration as seen in more chronic infections. However, rabbits are sensitive to anesthesia and thus cannot undergo imaging more than every 3 days. In a pilot experiment, rabbits with implants lacking the antibiotic coating were followed for 14 days, but this resulted in a more severe local OIAI causing unnecessary animal suffering (the rabbits no longer would use or bear weight on the infected leg) and all subsequent experiments were thus ended at 7 days. Our future work using this rabbit model of OIAI will address whether bacterial invasion and colonization of the osteocytic-canalicular network occurs as previously described[44-46] and will evaluate other antibiotic-release strategies for different infections, such as those involving indolent and gram-negative bacteria, as well as more chronic infections.

In conclusion, our findings provide proof of concept for combining a larger-animal model of OIAI with noninvasive in vivo BLI technology to potentially translate findings from preclinical animal models of OIAI to humans. ■

Robert J. Miller, MS[1]
John M. Thompson, MD[1]
Jesse Zheng, BS[2]
Mark C. Marchitto, MD[1]
Nathan K. Archer, PhD[1]
Bret L. Pinsker, BS[1]
Roger V. Ortines, MS[1]
Xuesong Jiang, PhD[2]
Russell A. Martin, PhD[2]
Isabelle D. Brown, BS[1]
Yu Wang, PhD[1]
Robert S. Sterling, MD[1]
Hai-Quan Mao, PhD[2]
Lloyd S. Miller, MD, PhD[1,2]

[1]Departments of Dermatology (R.J.M., M.C.M., N.K.A., B.L.P., R.V.O., I.D.B., Y.W., and L.S.M.) and Orthopaedic Surgery (J.M.T., R.S.S., and L.S.M.) and Division of Infectious Diseases, Department of Medicine (L.S.M.), Johns Hopkins University School of Medicine, Baltimore, Maryland

[2]Departments of Biomedical Engineering (J.Z.) and Materials Science and Engineering (X.J., R.A.M., H.-Q.M., and L.S.M.), Translational Tissue Engineering Center (X.J., R.A.M., H.-Q.M., and L.S.M.), Institute for

NanoBioTechnology (X.J., R.A.M., and H.-Q.M.), and Whitaker Biomedical Engineering Institute (H.-Q.M.), Johns Hopkins University, Baltimore, Maryland

E-mail address for L.S. Miller: lloydmiller@jhmi.edu

ORCID iD for R.J. Miller: 0000-0002-7662-6136
ORCID iD for J.M. Thompson: 0000-0002-7981-2882
ORCID iD for J. Zheng: 0000-0002-3713-4972
ORCID iD for M.C. Marchitto: 0000-0002-9136-1463
ORCID iD for N.K. Archer: 0000-0002-8212-8985
ORCID iD for B.L. Pinsker: 0000-0002-3811-4578
ORCID iD for R.V. Ortines: 0000-0001-9650-3072
ORCID iD for X. Jiang: 0000-0002-6564-6190
ORCID iD for R.A. Martin: 0000-0002-6483-6005
ORCID iD for I.D. Brown: 0000-0002-9313-7895
ORCID iD for Y. Wang: 0000-0002-4153-7360
ORCID iD for R.S. Sterling: 0000-0003-2963-3162
ORCID iD for H.-Q. Mao: 0000-0002-4262-9988
ORCID iD for L.S. Miller: 0000-0002-8332-2210

References

1. Del Pozo JL, Patel R. Clinical practice. Infection associated with prosthetic joints. N Engl J Med. 2009 Aug 20;361(8):787-94.

2. Osmon DR, Berbari EF, Berendt AR, Lew D, Zimmerli W, Steckelberg JM, Rao N, Hanssen A, Wilson WR; Infectious Diseases Society of America. Diagnosis and management of prosthetic joint infection: clinical practice guidelines by the Infectious Diseases Society of America. Clin Infect Dis. 2013 Jan;56(1):e1-25. Epub 2012 Dec 6.

3. Zimmerli W, Trampuz A, Ochsner PE. Prosthetic-joint infections. N Engl J Med. 2004 Oct 14;351(16):1645-54.

4. Cram P, Lu X, Kates SL, Singh JA, Li Y, Wolf BR. Total knee arthroplasty volume, utilization, and outcomes among Medicare beneficiaries, 1991-2010. JAMA. 2012 Sep 26;308(12):1227-36.

5. Kurtz SM, Lau E, Watson H, Schmier JK, Parvizi J. Economic burden of periprosthetic joint infection in the United States. J Arthroplasty. 2012 Sep; 27(8)(Suppl):61-5.e1. Epub 2012 May 2.

6. Wolf BR, Lu X, Li Y, Callaghan JJ, Cram P. Adverse outcomes in hip arthroplasty: long-term trends. J Bone Joint Surg Am. 2012 Jul 18;94(14):e103.

7. Craig J, Fuchs T, Jenks M, Fleetwood K, Franz D, Iff J, Raschke M. Systematic review and meta-analysis of the additional benefit of local prophylactic antibiotic therapy for infection rates in open tibia fractures treated with intramedullary nailing. Int Orthop. 2014 May;38(5):1025-30. Epub 2014 Feb 15.

8. Patzakis MJ, Wilkins J. Factors influencing infection rate in open fracture wounds. Clin Orthop Relat Res. 1989 Jun;243:36-40.

9. Darouiche RO. Treatment of infections associated with surgical implants. N Engl J Med. 2004 Apr 1;350(14):1422-9.

10. Kurtz SM, Ong KL, Lau E, Bozic KJ. Impact of the economic downturn on total joint replacement demand in the United States: updated projections to 2021. J Bone Joint Surg Am. 2014 Apr 16;96(8):624-30.

11. Kurtz S, Ong K, Lau E, Mowat F, Halpern M. Projections of primary and revision hip and knee arthroplasty in the United States from 2005 to 2030. J Bone Joint Surg Am. 2007 Apr;89(4):780-5.

12. Bernthal NM, Pribaz JR, Stavrakis AI, Billi F, Cho JS, Ramos RI, Francis KP, Iwakura Y, Miller LS. Protective role of IL-1β against post-arthroplasty Staphylococcus aureus infection. J Orthop Res. 2011 Oct;29(10):1621-6. Epub 2011 Mar 28.

13. Carli AV, Bhimani S, Yang X, Shirley MB, de Mesy Bentley KL, Ross FP, Bostrom MP. Quantification of peri-implant bacterial load and in vivo biofilm formation in an innovative, clinically representative mouse model of periprosthetic joint infection. J Bone Joint Surg Am. 2017 Mar 15;99(6):e25.

14. Dworsky EM, Hegde V, Loftin AH, Richman S, Hu Y, Lord E, Francis KP, Miller LS, Wang JC, Scaduto A, Bernthal NM. Novel in vivo mouse model of implant related spine infection. J Orthop Res. 2017 Jan;35(1):193-9. Epub 2016 May 8.

15. Hosman AH, Bulstra SK, Sjollema J, van der Mei HC, Busscher HJ, Neut D. The influence of Co-Cr and UHMWPE particles on infection persistence: an in vivo study in mice. J Orthop Res. 2012 Mar;30(3):341-7. Epub 2011 Aug 22.

16. Li D, Gromov K, Søballe K, Puzas JE, O'Keefe RJ, Awad H, Drissi H, Schwarz EM. Quantitative mouse model of implant-associated osteomyelitis and the kinetics of microbial growth, osteolysis, and humoral immunity. J Orthop Res. 2008 Jan;26(1): 96-105.

17. Nishitani K, Sutipornpalangkul W, de Mesy Bentley KL, Varrone JJ, Bello-Irizarry SN, Ito H, Matsuda S, Kates SL, Daiss JL, Schwarz EM. Quantifying the natural history of biofilm formation in vivo during the establishment of chronic implant-associated Staphylococcus aureus osteomyelitis in mice to identify critical pathogen and host factors. J Orthop Res. 2015 Sep;33(9):1311-9. Epub 2015 May 18.

18. Niska JA, Meganck JA, Pribaz JR, Shahbazian JH, Lim E, Zhang N, Rice BW, Akin A, Ramos RI, Bernthal NM, Francis KP, Miller LS. Monitoring bacterial burden, inflammation and bone damage longitudinally using optical and μCT imaging in an orthopaedic implant infection in mice. PLoS One. 2012;7(10):e47397. Epub 2012 Oct 17.

19. Pajarinen J, Lin TH, Sato T, Loi F, Yao Z, Konttinen YT, Goodman SB. Establishment of green fluorescent protein and firefly luciferase expressing mouse primary macrophages for in vivo bioluminescence imaging. PLoS One. 2015 Nov 10;10(11): e0142736.

20. Pribaz JR, Bernthal NM, Billi F, Cho JS, Ramos RI, Guo Y, Cheung AL, Francis KP, Miller LS. Mouse model of chronic post-arthroplasty infection: noninvasive in vivo bioluminescence imaging to monitor bacterial burden for long-term study. J Orthop Res. 2012 Mar;30(3):335-40. Epub 2011 Aug 11.

21. Romero Pastrana F, Thompson JM, Heuker M, Hoekstra H, Dillen CA, Ortines RV, Ashbaugh AG, Pickett JE, Linssen MD, Bernthal NM, Francis KP, Buist G, van Oosten M, van Dam GM, Thorek DLJ, Miller LS, van Dijl JM. Noninvasive optical and nuclear imaging of Staphylococcus-specific infection with a human monoclonal antibody-based probe. Virulence. 2018 Jan 1;9(1):262-72. Epub 2017 Dec 26.

22. Wang Y, Thompson JM, Ashbaugh AG, Khodakivskyi P, Budin G, Sinisi R, Heinmiller A, van Oosten M, van Dijl JM, van Dam GM, Francis KP, Bernthal NM, Dubikovskaya EA, Miller LS. Preclinical evaluation of photoacoustic imaging as a novel noninvasive approach to detect an orthopaedic implant infection. J Am Acad Orthop Surg. 2017 Feb;25(Suppl 1):S7-12.

23. Ashbaugh AG, Jiang X, Zheng J, Tsai AS, Kim WS, Thompson JM, Miller RJ, Shahbazian JH, Wang Y, Dillen CA, Ordonez AA, Chang YS, Jain SK, Jones LC, Sterling RS, Mao HQ, Miller LS. Polymeric nanofiber coating with tunable combinatorial antibiotic delivery prevents biofilm-associated infection in vivo. Proc Natl Acad Sci U S A. 2016 Nov 8;113(45):E6919-28. Epub 2016 Oct 24.

24. Bernthal NM, Stavrakis AI, Billi F, Cho JS, Kremen TJ, Simon SI, Cheung AL, Finerman GA, Lieberman JR, Adams JS, Miller LS. A mouse model of post-arthroplasty Staphylococcus aureus joint infection to evaluate in vivo the efficacy of antimicrobial implant coatings. PLoS One. 2010 Sep 7;5(9):e12580.

25. Hegde V, Dworsky EM, Stavrakis AI, Loftin AH, Zoller SD, Park HY, Richman S, Johansen D, Hu Y, Taylor JA, Hamad CD, Chun RF, Xi W, Adams JS, Bernthal NM. Single-dose, preoperative vitamin-D supplementation decreases infection in a mouse model of periprosthetic joint infection. J Bone Joint Surg Am. 2017 Oct 18; 99(20):1737-44.

26. Hu Y, Hegde V, Johansen D, Loftin AH, Dworsky E, Zoller SD, Park HY, Hamad CD, Nelson GE, Francis KP, Scaduto A, Bernthal NM. Combinatory antibiotic therapy increases rate of bacterial kill but not final outcome in a novel mouse model of Staphylococcus aureus spinal implant infection. PLoS One. 2017 Feb 28;12(2): e0173019.

27. Inzana JA, Schwarz EM, Kates SL, Awad HA. A novel murine model of established Staphylococcal bone infection in the presence of a fracture fixation plate to study therapies utilizing antibiotic-laden spacers after revision surgery. Bone. 2015 Mar;72:128-36. Epub 2014 Nov 29.

28. Niska JA, Shahbazian JH, Ramos RI, Francis KP, Bernthal NM, Miller LS. Vancomycin-rifampin combination therapy has enhanced efficacy against an experimental Staphylococcus aureus prosthetic joint infection. Antimicrob Agents Chemother. 2013 Oct;57(10):5080-6. Epub 2013 Aug 5.

29. Niska JA, Shahbazian JH, Ramos RI, Pribaz JR, Billi F, Francis KP, Miller LS. Daptomycin and tigecycline have broader effective dose ranges than vancomycin as prophylaxis against a Staphylococcus aureus surgical implant infection in mice. Antimicrob Agents Chemother. 2012 May;56(5):2590-7. Epub 2012 Feb 27.

30. Stavrakis AI, Zhu S, Hegde V, Loftin AH, Ashbaugh AG, Niska JA, Miller LS, Segura T, Bernthal NM. In vivo efficacy of a "smart" antimicrobial implant coating. J Bone Joint Surg Am. 2016 Jul 20;98(14):1183-9.

31. Thompson JM, Saini V, Ashbaugh AG, Miller RJ, Ordonez AA, Ortines RV, Wang Y, Sterling RS, Jain SK, Miller LS. Oral-only linezolid-rifampin is highly effective compared with other antibiotics for periprosthetic joint infection: study of a mouse model. J Bone Joint Surg Am. 2017 Apr 19;99(8):656-65.

32. Varrone JJ, de Mesy Bentley KL, Bello-Irizarry SN, Nishitani K, Mack S, Hunter JG, Kates SL, Daiss JL, Schwarz EM. Passive immunization with anti-glucosaminidase monoclonal antibodies protects mice from implant-associated osteomyelitis by mediating opsonophagocytosis of Staphylococcus aureus mega-clusters. J Orthop Res. 2014 Oct;32(10):1389-96. Epub 2014 Jul 3.

33. Wang Y, Cheng LI, Helfer DR, Ashbaugh AG, Miller RJ, Tzomides AJ, Thompson JM, Ortines RV, Tsai AS, Liu H, Dillen CA, Archer NK, Cohen TS, Tkaczyk C, Stover CK,

Sellman BR, Miller LS. Mouse model of hematogenous implant-related *Staphylococcus aureus* biofilm infection reveals therapeutic targets. Proc Natl Acad Sci U S A. 2017 Jun 27;114(26):E5094-102. Epub 2017 Jun 12.

34. Andreu N, Zelmer A, Wiles S. Noninvasive biophotonic imaging for studies of infectious disease. FEMS Microbiol Rev. 2011 Mar;35(2):360-94. Epub 2010 Oct 19.

35. Suhardi VJ, Bichara DA, Kwok S, Freiberg AA, Rubash H, Malchau H, Yun SH, Muratoglu OK, Oral E. A fully functional drug-eluting joint implant. Nat Biomed Eng. 2017;1:1. Epub 2017 Jun 13.

36. Gatin L, Saleh-Mghir A, Massin P, Crémieux AC. Critical analysis of experimental models of periprosthetic joint infection. Orthop Traumatol Surg Res. 2015 Nov; 101(7):851-5. Epub 2015 Oct 9.

37. Lovati AB, Bottagisio M, de Vecchi E, Gallazzi E, Drago L. Animal models of implant-related low-grade infections. a twenty-year review. Adv Exp Med Biol. 2017; 971:29-50.

38. Plaut RD, Mocca CP, Prabhakara R, Merkel TJ, Stibitz S. Stably luminescent Staphylococcus aureus clinical strains for use in bioluminescent imaging. PLoS One. 2013;8(3):e59232. Epub 2013 Mar 12.

39. Singh R, Ray P, Das A, Sharma M. Role of persisters and small-colony variants in antibiotic resistance of planktonic and biofilm-associated Staphylococcus aureus: an in vitro study. J Med Microbiol. 2009 Aug;58(Pt 8):1067-73. Epub 2009 Jun 15.

40. Darouiche RO, Mansouri MD, Zakarevicz D, Alsharif A, Landon GC. In vivo efficacy of antimicrobial-coated devices. J Bone Joint Surg Am. 2007 Apr;89(4):792-7.

41. Spaan AN, van Strijp JAG, Torres VJ. Leukocidins: staphylococcal bi-component pore-forming toxins find their receptors. Nat Rev Microbiol. 2017 Jul;15(7):435-47. Epub 2017 Apr 19.

42. Dash TK, Konkimalla VB. Poly-ε-caprolactone based formulations for drug delivery and tissue engineering: a review. J Control Release. 2012 Feb 28;158(1): 15-33.

43. Jain RA. The manufacturing techniques of various drug loaded biodegradable poly(lactide-co-glycolide) (PLGA) devices. Biomaterials. 2000 Dec;21(23):2475-90.

44. de Mesy Bentley KL, MacDonald A, Schwarz EM, Oh I. Chronic osteomyelitis with Staphylococcus aureus deformation in submicron canaliculi of osteocytes: a case report. JBJS Case Connect. 2018 Jan-Mar;8(1):e8.

45. de Mesy Bentley KL, Trombetta R, Nishitani K, Bello-Irizarry SN, Ninomiya M, Zhang L, Chung HL, McGrath JL, Daiss JL, Awad HA, Kates SL, Schwarz EM. Evidence of Staphylococcus aureus deformation, proliferation, and migration in canaliculi of live cortical bone in murine models of osteomyelitis. J Bone Miner Res. 2017 May; 32(5):985-90. Epub 2017 Jan 26.

46. Yang D, Wijenayaka AR, Solomon LB, Pederson SM, Findlay DM, Kidd SP, Atkins GJ. Novel insights into Staphylococcus aureus deep bone infections: the involvement of osteocytes. MBio. 2018 Apr 24;9(2):e00415-18.